

Equilibrium Propagation for Non-Conservative Systems

Antonino Emanuele Scurria¹ Dimitri Vanden Abeele¹ Bortolo Matteo Mognetti² Serge Massar¹

Abstract

Equilibrium Propagation (EP) is a physics-inspired learning algorithm that uses stationary states of a dynamical system both for inference and learning. In its original formulation it is limited to conservative systems, *i.e.* to dynamics which derive from an energy function. Given their importance in applications, it is important to extend EP to nonconservative systems, *i.e.* systems with non-reciprocal interactions. Previous attempts to generalize EP to such systems failed to compute the exact gradient of the cost function. Here we propose a framework that extends EP to arbitrary nonconservative systems, including feedforward networks. We keep the key property of equilibrium propagation, namely the use of stationary states both for inference and learning. However, we modify the dynamics in the learning phase by a term proportional to the non-reciprocal part of the interaction so as to obtain the exact gradient of the cost function. This algorithm can also be derived using a variational formulation that generates the learning dynamics through an energy function defined over an augmented state space. Numerical experiments using the MNIST database show that this algorithm achieves better performance and learns faster than previous proposals.

1. Introduction

Standard neural network optimization relies on error backpropagation, an algorithm whose computational mechanism is difficult to reconcile with biological (Crick, 1989) and physical implementations (Indiveri & Liu, 2015). Specifically, backpropagation requires a backward pass distinct from inference, the transmission of nonlocal error signals,

¹Laboratoire d’Information Quantique (LIQ) CP224, Université libre de Bruxelles (ULB), Av. F. D. Roosevelt 50, 1050 Bruxelles, Belgium ²Interdisciplinary Center for Nonlinear Phenomena and Complex Systems CP231, Université libre de Bruxelles (ULB), Av. F. D. Roosevelt 50, 1050 Bruxelles, Belgium. Correspondence to: Antonino Emanuele Scurria <antonino.scurria@ulb.be>.

Preprint. February 4, 2026.

and synchronous layer-wise computations with explicit gradient storage. These constraints have no clear analog in physical systems, making backpropagation challenging to implement in neuromorphic or analog hardware. Consequently, understanding how credit assignment can instead emerge from intrinsic system dynamics, through local interactions and continuous relaxation, is a central question in neuroscience and machine learning.

Equilibrium Propagation (EP) (Scellier & Bengio, 2017) represents one of the most promising advances in this direction. It formulates supervised learning as a contrast between two stationary states of a dynamical system: a ‘free’ phase where the system evolves autonomously, and a ‘nudged’ phase where outputs are weakly pushed toward their targets. In energy-based dynamics, the local change in neural states between these phases recovers the exact gradient of the cost function with respect to parameters. This enables spatially local learning exploiting the continuous relaxation of the system without a distinct backward circuit or explicit weight transport.

Since its introduction, several works have sought to improve the practicality and biological realism of EP. Algorithmic adaptations include enforcing temporal locality to avoid state storage (Ernoult et al., 2020; Falk et al., 2025), deriving agnostic updates for black-box energies (Scellier et al., 2022), and substituting nudging with clamping (Stern et al., 2021). Theoretically, the framework has been extended to stochastic systems (Scellier & Bengio, 2017; Massar & Mognetti, 2025) and Lagrangian dynamics for time-varying inputs (Massar, 2025; Pourcel et al., 2025; Berneman & Hexner, 2025). In parallel, simulations have explored suitable substrates, ranging from spiking (Martin et al., 2021; O’Connor et al., 2019) and resistive networks (Kendall et al., 2020) to coupled oscillators (Wang et al., 2024; Rageau & Grollier, 2025), as well as quantum systems (Wanjura & Marquardt, 2025; Massar & Mognetti, 2025; Scellier, 2024). Finally, experimental realizations have been demonstrated in memristor crossbars (Yi et al., 2023), self-adjusting electrical circuits (Dillavou et al., 2022; 2024), elastic networks (Altman et al., 2024), and classical Ising models trained on quantum annealers (Laydevant et al., 2024).

Despite these recent developments and the theoretical el-

egance of EP, its standard formulation remains restricted to conservative systems. In these systems, dynamics are derived from an energy function, which inherently enforces symmetry (*e.g.*, symmetric synaptic connections $J_{ij} = J_{ji}$) through the action-reaction principle. This constraint precludes the use of EP in a broad class of models characterized by non-conservative forces. This includes the feedforward architectures dominant in modern AI and biological circuits which are generally asymmetric, as well as physical systems that reach stationary states far from thermodynamic equilibrium, such as nonlinear optical systems driven by external lasers (Cin et al., 2025), optoelectronic systems (Kalinin et al., 2025), exciton-polariton condensates (Sajnok & Matuszewski, 2025), active metamaterials (Brandenbourger et al., 2019) and active colloids (Bishop et al., 2023) (see (Bowick et al., 2022) for a comprehensive review).

Formally, we consider a dynamical system governed by a non-reciprocal force field $F(x, \theta, u)$, which relaxes to a stationary configuration \bar{x}^0 satisfying:

$$F(\bar{x}^0, \theta, u) = 0, \quad (1)$$

where x represents the state variables, θ the learnable parameters and u the static input. Our goal, given a target $y(u)$, is to compute the gradient of the cost function $C(\bar{x}^0, y)$ at this equilibrium,

$$\frac{dC}{d\theta}(\bar{x}^0, y), \quad (2)$$

and update θ to minimize the cost.

Previous attempts to extend EP to non-conservative dynamics include the *Vector Field* (VF) algorithm (Scellier et al., 2018). However, as noted by the authors, this method provides an unbiased gradient of the cost Eq. (2) only in the conservative case. To mitigate this, (Laborieux & Zenke, 2024) proposed adding a penalty to keep the Jacobian close to symmetry, essentially forcing the system to be as conservative as possible. Alternative methods related to VF, which similarly do not compute the exact gradient, were proposed in (Farinha et al., 2020; Costa & Santos, 2025) and for specific systems in simulation (Cin et al., 2025; Sajnok & Matuszewski, 2025).

Conversely, generalizations of backpropagation can handle non-reciprocal forces and compute the exact gradient of the cost Eq. (2) but inherit the same challenges in physical implementations. For instance, Backpropagation Through Time (Werbos, 2002) unfolds the network in time to apply standard backpropagation, Recurrent Backpropagation (Almeida, 1990; Pineda, 1987) avoids this memory requirement but still requires a specific circuit to propagate errors, and the continuous Adjoint Method (Chen et al., 2018) additionally requires integrating the dynamics backward in time which is not physically possible for a dissipative system.

In this paper, we first propose *Asymmetric EP* (AEP), a

framework where the original dynamics serve for inference, while a new augmented dynamic is used to compute gradients of the cost Eq. (2). In this augmented phase, the output neurons are nudged towards their targets (as in standard EP), while a local corrective term – proportional to the antisymmetric part of the Jacobian at the free equilibrium $\mathcal{J}_F(\bar{x}^0, \theta, u) = \frac{\partial}{\partial x} F(\bar{x}^0, \theta, u)$ – is added to the forces. The exact gradients of the cost with respect to parameters are then obtained by contrasting stationary states of the augmented system.

Second, we introduce *Dyadic EP*, a ‘variational’ approach to learning in non-conservative systems. This method involves doubling the number of variables in the system’s state space and subsequently introducing a new energy function in this extended space. While applying the standard update rule of EP to this energy theoretically yields the exact gradients, we present an optimized implementation. Dyadic EP takes advantage of the extended space to execute the positive and negative nudging phases in parallel, recovering the same computational cost as AEP. Derived from first principles, this approach is inspired by established methods for mapping dissipative dynamical systems onto conservative ones by doubling the degrees of freedom (Bateman, 1931; Galley, 2013; Aykroyd et al., 2025). It is related to the Dual Propagation algorithm introduced in (Høier et al., 2023) which can be viewed as Dyadic EP restricted to the specific case of a symmetric (conservative) layered coupling matrix.

Finally, we validate our framework on MNIST (LeCun, 1998). In continuous Hopfield networks initialized with symmetric connection matrices, AEP achieves better accuracy and learns faster than EP and VF. Additionally, when we constrain the network to have a strong degree of structural asymmetry, in which case EP is inapplicable, AEP considerably outperforms VF. Finally, when we restrict connections to a feedforward structure, our algorithm effectively trains all parameters; in contrast, VF is limited to training the last layer, acting essentially as an Extreme Learning Machine (Huang et al., 2006; Wang et al., 2022) with poor performance.

In summary, this theoretical work proposes two generalizations of EP beyond conservative systems to arbitrary differentiable dynamics that compute in their stationary states.

2. Equilibrium Propagation Overview

2.1. Conservative Systems

We first review standard *Equilibrium Propagation* (EP) (Scellier & Bengio, 2017). We consider a network described by an energy function $E(x, \theta, u)$, such that the force field is derived from the potential E :

$$F_E(x, \theta, u) = -\frac{\partial}{\partial x} E(x, \theta, u). \quad (3)$$

The objective is to compute the total gradient $\frac{dC}{d\theta}(\bar{x}^0, y)$ of a (quadratic) cost function $C(x, y)$ evaluated at the minimum energy configuration of the system. This *free equilibrium* denoted \bar{x}^0 (which depend implicitly in θ and u), satisfies the stationarity condition:

$$-\frac{\partial}{\partial x} E(\bar{x}^0, \theta, u) = 0. \quad (4)$$

To compute gradients, we then introduce the augmented energy functional:

$$E_T(x, \theta, \beta, u, y) = E(x, \theta, u) + \beta C(x, y), \quad (5)$$

where β is a scalar nudging parameter. The stationary configuration of this augmented system is obtained by integrating the dynamics

$$\frac{dx}{dt} = -\frac{\partial E_T(x, \theta, \beta, u)}{\partial x}, \quad (6)$$

until the energy minimum is reached. This new fixed point \bar{x}^β , called *nudged equilibrium*, satisfies:

$$\frac{\partial E(\bar{x}^\beta, \theta, u)}{\partial x} + \beta \frac{\partial C(\bar{x}^\beta, y)}{\partial x} = 0. \quad (7)$$

The training procedure, as improved in (Laborieux et al., 2021), uses two nudged phases with factors $\pm\beta$ (with $\beta \neq 0$). Starting from \bar{x}^0 , the system relaxes to two nearby perturbed equilibria, $\bar{x}^{+\beta}$ and $\bar{x}^{-\beta}$. The displacement $\bar{x}^{+\beta} - \bar{x}^{-\beta}$ is then used to compute the parameter update in the learning rule:

$$\Delta\theta = -\epsilon \frac{1}{2\beta} \left(\frac{\partial E(\bar{x}^\beta, \theta, u)}{\partial \theta} - \frac{\partial E(\bar{x}^{-\beta}, \theta, u)}{\partial \theta} \right), \quad (8)$$

where $\epsilon > 0$ is the learning rate. The theoretical foundation of EP is the result that, in the $\lim_{\beta \rightarrow 0}$ of Eq. (8) we get:

$$\frac{dC(\bar{x}^0, y)}{d\theta} = \frac{d}{d\beta} \frac{\partial E(\bar{x}^\beta, \theta, u)}{\partial \theta}, \quad (9)$$

see Appendix C.1. The error of the above method is $O(\beta^2)$. This error can be further reduced using holomorphic equilibrium propagation (Laborieux & Zenke, 2022).

Thus, EP recovers the exact gradient of the cost function using only local computations for an appropriate energy functional E . In this manner, learning implements gradient descent without an explicit backward pass, and credit assignment is realized through the system's intrinsic relaxation dynamics.

Three remarks can be made at this point. First, EP does not require the system to be at an energy minimum, but only at a stationary point, *i.e.*, that Eq. (7) holds. Second, EP implicitly assumes that the Jacobian $\mathcal{J}_E(\bar{x}^0, u) = \frac{\partial}{\partial x} F_E(\bar{x}^0, u)$ is invertible. In this work, we assume this condition holds and will not state it explicitly hereafter. Third, for simplicity, we omit the dependency on the input u and target y in the following equations.

2.2. Vector Field

The *Vector Field* (VF) algorithm, introduced in (Scellier et al., 2018), is an early attempt to adapt EP to non-reciprocal forces. This method relies on the observation that, for conservative systems, linearizing the right-hand side of Eq. (9) around the equilibrium point \bar{x}^0 yields

$$\begin{aligned} \lim_{\beta \rightarrow 0} \frac{1}{2\beta} \left(\frac{\partial E(\bar{x}^\beta, \theta)}{\partial \theta} - \frac{\partial E(\bar{x}^{-\beta}, \theta)}{\partial \theta} \right) \\ = \lim_{\beta \rightarrow 0} \left(-\frac{\partial F_E}{\partial \theta}(\bar{x}^0, \theta) \right)^\top \left(\frac{\bar{x}^\beta - \bar{x}^{-\beta}}{2\beta} \right), \end{aligned} \quad (10)$$

where $F_E = -\partial_x E(x, \theta)$ is the conservative force. It is therefore tempting to use the right-hand side of Eq. (10) for parameter updates of non-conservative systems, where no energy function E exists.

The VF algorithm adopts precisely this approach. It uses the nudged counterpart of Eq. (7),

$$F(\bar{x}^\beta, \theta) - \beta \frac{\partial C}{\partial x}(\bar{x}^\beta) = 0, \quad (11)$$

in conjunction with the learning rule:

$$\Delta\theta = \epsilon \left(\frac{\partial F}{\partial \theta}(\bar{x}^0, \theta) \right)^\top \left(\frac{\bar{x}^\beta - \bar{x}^{-\beta}}{2\beta} \right). \quad (12)$$

However, as noted in (Scellier et al., 2018), Eq. (12) does not align with the true gradient $\frac{dC}{d\theta}(\bar{x}^0)$ and is exact only if the force is conservative. To see this, let $\mathcal{J}_F(x, \theta)$ denote the Jacobian of the vector field $F(x, \theta)$ (in components $(\mathcal{J}_F(x, \theta))_{ij} = \frac{\partial F_i(x, \theta)}{\partial x_j}$). Differentiating the equilibrium condition $F(\bar{x}^0, \theta) = 0$ with respect to θ gives

$$\mathcal{J}_F(\bar{x}^0, \theta) \frac{d\bar{x}^0}{d\theta} + \frac{\partial F}{\partial \theta}(\bar{x}^0, \theta) = 0. \quad (13)$$

Consequently, the exact gradient of the cost is

$$\begin{aligned} \frac{dC}{d\theta}(\bar{x}^0) &= \frac{d\bar{x}^0}{d\theta}^\top \frac{\partial C}{\partial x}(\bar{x}^0) \\ &= - \underbrace{\left(\frac{\partial F}{\partial \theta}(\bar{x}^0, \theta) \right)^\top}_{\text{pre-synaptic}} \underbrace{\left((\mathcal{J}_F^\top(\bar{x}^0, \theta))^{-1} \frac{\partial C}{\partial x}(\bar{x}^0) \right)}_{\text{post-synaptic}}. \end{aligned} \quad (14)$$

The terms ‘pre-synaptic’ and ‘post-synaptic’ in Eq. (14) are used by analogy with neuronal transmission. The pre-synaptic factor captures the local influence of the parameter θ on the force F , acting as a modulation of the incoming signal at the synapse. The post-synaptic factor represents the sensitivity of the cost to state perturbations, back-propagated through the linearized dynamics around the equilibrium.

This term quantifies how local synaptic changes impact the cost via the system's response.

If instead we differentiate the nudged equilibrium condition in Eq. (11) with respect to β and evaluate at $\beta = 0$, we obtain

$$\mathcal{J}_F(\bar{x}^0, \theta) \frac{d\bar{x}^\beta}{d\beta} \Big|_{\beta=0} - \frac{\partial C}{\partial x}(\bar{x}^0) = 0, \quad (15)$$

which gives

$$\frac{d\bar{x}^\beta}{d\beta} \Big|_{\beta=0} = (\mathcal{J}_F(\bar{x}^0, \theta))^{-1} \frac{\partial C}{\partial x}(\bar{x}^0, y). \quad (16)$$

The right-hand side of Eq. (16) represents the effective post-synaptic term used by the VF algorithm (Eq. 12). Comparing this with the exact post-synaptic term derived in Eq. (14), we see that they coincide only if $\mathcal{J}_F = \mathcal{J}_F^\top$, *i.e.*, only if the system is conservative.

Now, let $S_{\mathcal{J}}(\bar{x}^0, \theta)$ and $A_{\mathcal{J}}(\bar{x}^0, \theta)$ denote the symmetric and antisymmetric parts of the Jacobian at the free (un-nudged) equilibrium, respectively. Then, we show in Appendix A that the gradient error increases with the spectral radius of $(S_{\mathcal{J}}(\bar{x}^0, \theta))^{-1} A_{\mathcal{J}}(\bar{x}^0, \theta)$. Consequently, large antisymmetric contributions degrade the gradient estimation, confirming empirical observations in the Appendix of (Ernoult et al., 2020). In fact, in the pathological limit where the Jacobian would be purely antisymmetric $S_{\mathcal{J}}(\bar{x}^0, \theta) = 0$, the update of VF gives the negative of the true gradient, maximizing the cost rather than minimizing it.

3. Asymmetric EP

Here, we introduce *Asymmetric EP* (AEP), see Algorithm 1, which corrects the gradient estimate error inherent to VF by adding a local correction term to the augmented inference dynamics. The new nudged equilibrium \bar{x}_A^β satisfies:

$$F(\bar{x}_A^\beta, \theta) - \beta \frac{\partial C}{\partial x}(\bar{x}_A^\beta) - 2A_{\mathcal{J}}(\bar{x}^0, \theta)(\bar{x}_A^\beta - \bar{x}^0) = 0, \quad (22)$$

As in VF, we then obtain two perturbed states $\bar{x}_A^{\pm\beta}$ for opposite nudging $\pm\beta$ and apply the contrastive learning rule of Eq. (12)

We now show that AEP gives rise to the correct learning rule, *i.e.* that right-hand side of Eq. (21) is proportional to the gradient of the cost function $\frac{dC}{d\theta}(\bar{x}^0)$ at the equilibrium point \bar{x}^0 (Eq. 14). To this end, note that the same reasoning leading to Eq. (16) leads to

$$\frac{d\bar{x}_A^\beta}{d\beta} \Big|_{\beta=0} = (\mathcal{J}_{F_A}(\bar{x}^0, \theta))^{-1} \frac{\partial C}{\partial x}(\bar{x}^0). \quad (23)$$

where $\mathcal{J}_{F_A}(x, \theta)$ is the Jacobian of the modified dynamical system Eq. (20). At the equilibrium point \bar{x}^0 , \mathcal{J}_{F_A} is equal

Algorithm 1 Asymmetric EP (AEP)

- 1: **Inputs:** Force field $F(x, \theta)$, cost function $C(x)$, nudging parameter β , learning rate ϵ .
- 2: **repeat**
- 3: **1. Free Phase: Evolve to stationary state**
- 4: Evolve the system dynamics
- 5: $\frac{dx}{dt} = F(x, \theta),$ (17)
- 6: until convergence to the stationary state $\bar{x}^0.$
- 7: **2. Jacobian Decomposition**
- 8: Compute the Jacobian at equilibrium:
- 9: $\mathcal{J}_F(\bar{x}^0, \theta) = \frac{\partial F}{\partial x}(\bar{x}^0, \theta),$ (18)
- 10: and decompose it in its antisymmetric part:
- 11:
- 12: **3. Nudged Phase: Augmented Dynamics**
- 13: Integrate the dynamics twice starting from \bar{x}^0
- 14: $\frac{dx}{dt} = F(x, \theta) - \beta \frac{\partial C}{\partial x}(x) - 2A_{\mathcal{J}}(\bar{x}^0, \theta)(x - \bar{x}^0),$ (20)
- 15: until convergence to two new stationary states $\bar{x}_A^{\pm\beta}.$
- 16: **4. Parameter Update**
- 17: Update the parameters according to:
- 18:
- 19: **until** convergence of θ
- 20: **Output:** Optimized parameters $\theta.$

to the transpose of the original Jacobian:

$$\begin{aligned} \mathcal{J}_{F_A}(\bar{x}^0, \theta) &= \mathcal{J}_F(\bar{x}^0, \theta) - 2A_{\mathcal{J}}(\bar{x}^0, \theta) \\ &= S_{\mathcal{J}}(\bar{x}^0, \theta) - A_{\mathcal{J}}(\bar{x}^0, \theta) \\ &= \mathcal{J}_F^\top(\bar{x}^0, \theta). \end{aligned} \quad (24)$$

where we have used the decomposition Eq. (43) of \mathcal{J} the original Jacobian into its symmetric and antisymmetric components. Therefore, the left hand side of Eq. (23) is equal to the true post-synaptic term

$$\frac{d\bar{x}_A^\beta}{d\beta} \Big|_{\beta=0} = (\mathcal{J}_F^\top(\bar{x}^0, \theta))^{-1} \frac{\partial C}{\partial x}(\bar{x}^0), \quad (25)$$

which, using Eq. (14), proves the result. Additionally, although implied by their convergence to the true gradient,

we explicitly demonstrate the equivalence of the gradient estimates obtained by AEP and Backpropagation Through Time in Appendix B using (Ernoult et al., 2019).

Finally, it is important to notice that the corrective term $-2A_J(\bar{x}^0, \theta)(x - \bar{x}^0)$ in Eq. (20) is spatially local. Indeed, $A_J(x^0, \theta)$ is zero for unconnected neurons, and $(x - \bar{x}^0)$ is available at the synapse level assuming that the memory mechanism already required for the learning rule (Eq. 12) is present. Mathematically, this correction can create backward connections, as explained in the simple feedforward case in Section 5.3. However, in neuromorphic realizations, both feedforward and corresponding feedback connections will need to be both physically present, even if, for instance, feedback connections can be deactivated during inference.

4. Dyadic EP

We now introduce *Dyadic EP* (Algorithm 2) an alternative ‘variational’ algorithm that computes the exact cost gradient in the limit of infinitesimal nudging, recovering the results of AEP via a conceptually distinct approach. Specifically, Dyadic EP maps the original n -variable dynamics governed by the force field $F(x, \theta)$ to a new system of $2n$ variables, z and z' , defined by an energy functional $H(z, z', \theta)$ and a cost $D(z, z')$.

We emphasize that this variable doubling is essential to constructing a potential for non-conservative forces. Without extending the configuration space, it is impossible to define a scalar generator for the dynamics, as the rotational component of a non-conservative field cannot be expressed as the gradient of a potential.

The new system is defined by the energy H and cost function D , given in terms of F and C by:

$$\begin{aligned} H(z, z', \theta) &= -(z - z')^\top F\left(\frac{z + z'}{2}, \theta\right), \\ D(z, z') &= C\left(\frac{z + z'}{2}\right), \end{aligned} \quad (26)$$

where $z, z' \in \mathbb{R}^n$. In order to learn, we introduce the augmented energy

$$H_T(z, z', \theta, \beta) = H(z, z', \theta) + \beta D(z, z'). \quad (27)$$

The equilibrium configuration corresponds to a saddle point of H_T , where z minimizes and z' maximizes the energy. This poses no issue for EP, which requires only that the joint state (z, z') reaches a stationary state. Although this min-maximization can be interpreted as z evolving forward and z' backward in time, in practice evolve forward simulta-

neously, as we integrate the coupled equations:

$$\begin{aligned} \frac{dz}{dt} &= -\frac{\partial H_T}{\partial z} = F\left(\frac{z + z'}{2}, \theta\right) \\ &\quad + \left(\frac{z - z'}{2}\right)^\top \frac{\partial F}{\partial z}\bigg|_{\frac{z+z'}{2}} - \frac{\beta}{2} \frac{\partial C}{\partial z}\left(\frac{z + z'}{2}\right), \\ \frac{dz'}{dt} &= +\frac{\partial H_T}{\partial z'} = F\left(\frac{z + z'}{2}, \theta\right) \\ &\quad - \left(\frac{z - z'}{2}\right)^\top \frac{\partial F}{\partial z'}\bigg|_{\frac{z+z'}{2}} + \frac{\beta}{2} \frac{\partial C}{\partial z'}\left(\frac{z + z'}{2}\right), \end{aligned} \quad (28)$$

until a stationary point $(\bar{z}^\beta, \bar{z}'^\beta)$ is reached. Upon convergence, we follow the standard EP paradigm, using the difference $\bar{z}^\beta - \bar{z}'^\beta$ to compute the post-synaptic term. To understand why this works, consider the change of variables $m = (z + z')/2$ and $d = z - z'$. In Appendix C, we prove that m evolves according to the original dynamics F , ensuring valid inference. Meanwhile, the difference d acts as a “physical” error signal: it relaxes to a state proportional to the cost gradient, effectively performing backpropagation through the system’s intrinsic dynamics. This allows the energy H to generate exact gradients for non-conservative forces.

It is important to notice that while Dyadic EP introduces a distinct formulation, it remains consistent with the general theoretical setting of EP and matches the computational cost of AEP. Note also that we start the evolution of the free phase ($\beta = 0$) with the identical initial condition for z and z' , (i.e., $d = 0$). This guarantees that integrating Eq. (32) leads to a symmetric stationary point where $\bar{z}^0 = \bar{z}'^0$. Finally, we underline that the modified variational update rule in Eq. (34) is equivalent to the standard symmetric EP update rule in Eq. (8) (see Appendix C).

Now, to make this concrete, consider a continuous Hopfield network (see also Eq. (35)) with an asymmetric connection matrix J . After some calculations (see Appendix D), the augmented energy of the system can be re-expressed as:

$$\begin{aligned} H_T &= -\frac{1}{2} \rho(z)^\top S \rho(z) + \frac{1}{2} \rho(z')^\top S \rho(z') - \rho(z)^\top A \rho(z') \\ &\quad + \frac{1}{2} (\|z\|^2 - \|z'\|^2) + \frac{\beta}{2} (C(z, y) + C(z', y)), \end{aligned} \quad (29)$$

where S and A are the symmetric and antisymmetric parts of J , respectively and ρ is an element-wise non-linearity. An interesting analogy can be drawn with standard learning rules in discrete Hopfield networks (Hopfield, 1982). For a sequence of binary memories $\{\xi^1, \dots, \xi^m\}$ where $\xi^\mu \in \{-1, 1\}^n$, S corresponds to the standard autoassociative Hebbian rule $\sum_\mu \xi^\mu (\xi^\mu)^\top$, creating stable attractors at each pattern. In contrast, A corresponds to the heteroassociative rule (e.g., a cycle between ξ^μ and ξ^ν given by $\xi^\nu (\xi^\mu)^\top -$

$\xi^\mu(\xi^\nu)^\top$), encoding transitions between patterns.

For this specific energy, the update rule given by Eq. (34) can be re-expressed as:

$$\Delta J \propto -\frac{1}{2\beta} (\rho(\bar{z}'^\beta) - \rho(\bar{z}^\beta)) [\rho(\bar{z}'^\beta) + \rho(\bar{z}^\beta)]^\top. \quad (30)$$

In the limit $\beta \rightarrow 0$, this gives:

$$\Delta J \propto \left(\frac{\bar{d}^\beta}{\beta} \right) \odot \rho'(\bar{m}) \rho(\bar{m})^\top. \quad (31)$$

matching the learning rule in (Pineda, 1987), with $\lim_{\beta \rightarrow 0} \frac{\bar{d}^\beta}{\beta}$ being the error signal.

Algorithm 2 Dyadic EP

- 1: **Inputs:** Force field $F(x, \theta)$, cost function $C(x, y)$, nudging parameter β , learning rate ϵ
- 2: **repeat**
- 3: **1. Free Phase: Evolve to stationary state**
- 4: Evolve the system dynamics, starting from identical initial conditions $z(0) = z'(0) = z_0$,
- 5:
$$\begin{cases} \frac{dz}{dt} = -\frac{\partial H}{\partial z} \\ \frac{dz'}{dt} = +\frac{\partial H}{\partial z'} \end{cases} \quad (32)$$
- 6: until stationary states \bar{z}^0, \bar{z}'^0 are reached.
- 7: **2. Nudged Equilibrium**
- 8: Evolve the system dynamics, starting from the solution of the free phase $\bar{z}^0 = \bar{z}'^0$:
- 9:
$$\begin{cases} \frac{dz}{dt} = -\frac{\partial H_T}{\partial z} \\ \frac{dz'}{dt} = +\frac{\partial H_T}{\partial z'} \end{cases} \quad (33)$$
- 10: until two nudged stationary states $\bar{z}^\beta, \bar{z}'^\beta$ are reached.
- 11: **3. Parameter Update**
- 12: Update the parameters according to:
- 13:
$$\Delta\theta = -\epsilon \frac{1}{\beta} \left(\frac{\partial H(\bar{z}^\beta, \bar{z}'^\beta, \theta)}{\partial \theta} \right) \quad (34)$$
- 14: **until** convergence of θ
- 15: **Output:** Optimized parameters θ .

5. Numerical Experiments

In this section, we numerically validate AEP (Algorithm 1). The neuronal dynamics follows the one introduced in (Scellier & Bengio, 2017), and is generalized to allow for non-reciprocal forces as in (Scellier et al., 2018). For clarity,

we express the forces in a form that explicitly separates the contributions of the external input and the recurrent interactions:

$$F(x) = \rho'(x) \odot (J^{\text{in}}u + J^{\text{dyn}}\rho(x)) - x, \quad (35)$$

where $u \in \mathbb{R}^{N_{\text{in}}}$ denotes the input and $x \in \mathbb{R}^{N_{\text{dyn}}}$ the neuronal state, comprising both hidden and output units. The matrices $J^{\text{in}} \in \mathbb{R}^{N_{\text{dyn}} \times N_{\text{in}}}$ and $J^{\text{dyn}} \in \mathbb{R}^{N_{\text{dyn}} \times N_{\text{dyn}}}$ define the input and recurrent connectivity, respectively. The activation function $\rho(\cdot)$ is taken to be the hyperbolic tangent, applied element-wise.

If J^{dyn} is symmetric, we can define the energy:

$$E(x) = \frac{1}{2} \|x\|^2 - \frac{1}{2} \rho(x)^\top J^{\text{dyn}} \rho(x) - \rho(x)^\top J^{\text{in}} u, \quad (36)$$

which is identical to that of (Scellier & Bengio, 2017), provided that the input neurons are activated as $\rho(u)$.

Equation (35) naturally motivates a quantitative measure of structural asymmetry r_{str} , defined as:

$$r_{\text{str}} = \frac{\|(J^{\text{dyn}}^\top - J^{\text{dyn}})/2\|_F}{\|J^{\text{dyn}}\|_F}, \quad (37)$$

where $\|\cdot\|_F$ denotes the Frobenius norm. Note that this metric does not capture the asymmetry of the Jacobian, which depends on the state x .

For numerical experiments, we restricted the network to a layered architecture with a single hidden layer to facilitate comparison with prior work. Accordingly, J^{in} contains only input-to-hidden connections, while J^{dyn} is block off-diagonal, encoding bidirectional interactions between the hidden and output layers. Both J^{in} and J^{dyn} are trained.

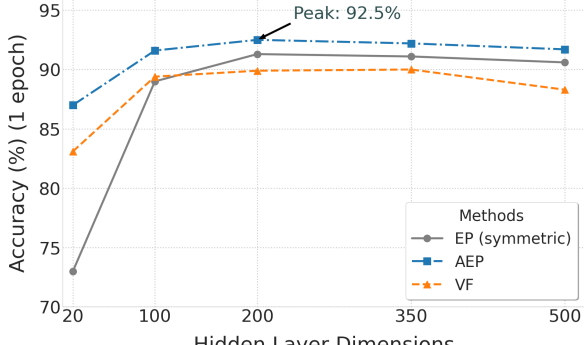
Following previous work, we use the MNIST dataset (Le-Cun, 1998) (60k train, 10k test), with inputs normalized using min-max to $[-1, 1]$ and one-hot targets in $\{-1, 1\}$. All hyperparameters are detailed in Appendix F, along with additional technical details and numerical results.

5.1. Symmetric Initialization

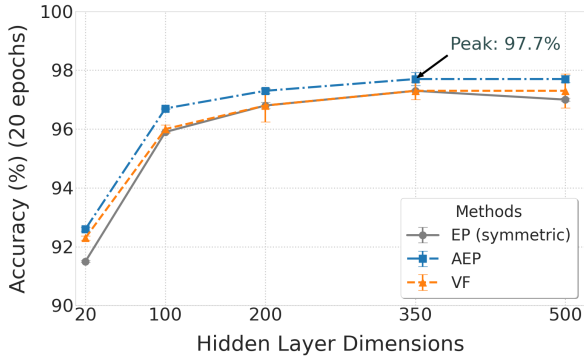
We start by comparing AEP with standard EP and VF. All methods are initialized with an identical symmetric matrix J^{dyn} . EP maintains this symmetry throughout training, while VF and AEP naturally induce asymmetry in J^{dyn} .

Since EP and VF already achieve strong performance on MNIST, the purpose of this experiment is to validate AEP and compare it against these baselines rather than outperform the state of the art.

Figure 1 compares the performance of the three algorithms as a function of the dimension of the hidden layer after 1 and 20 epochs. AEP consistently outperforms the baselines in accuracy, suggesting that it learns faster and better.



(a) Results after one epoch.



(b) Results after 20 epochs.

Figure 1. Comparison of algorithm performance on MNIST using a layered architecture with one hidden layer and symmetric initialization. Squares denote AEP, circles EP, and triangles VF. Test accuracy (averaged over 10 runs) is shown after one epoch (Fig. 1a) and 20 epochs (Fig. 1b).

Figure 2 studies the evolution of the asymmetry ratio r_{str} . The results are reported for 50 hidden neurons. As expected, EP preserves the initial weight symmetry. In contrast, VF and AEP induce non-trivial evolution of r_{str} following two distinct patterns, resulting in three distinct network configurations. A complementary figure is available in Appendix F.1.

5.2. Fixed Asymmetry Ratio

While the previous section focused on networks compatible with all three algorithms (EP, VF, AEP), we now turn to architectures with strong structural asymmetry. In this regime, EP is inapplicable by construction, and, as we show, VF performs poorly, contrary to AEP which remains effective.

To this end, we consider a class of networks where the asymmetry ratio r_{str} defined in Eq. (37) is kept fixed. Let \tilde{S} and \tilde{A} be arbitrary symmetric and antisymmetric matrices in $\mathbb{R}^{N_{\text{dyn}} \times N_{\text{dyn}}}$. We enforce a fixed r_{str} via the

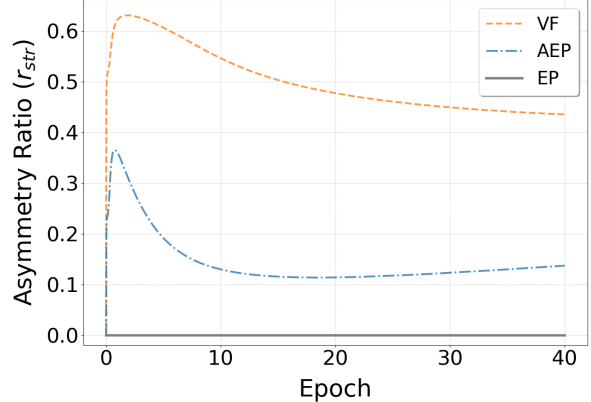


Figure 2. Evolution of the asymmetry ratio r_{str} (defined in Eq. (37)) during training on MNIST for AEP, EP, and VF, initialized from a symmetric configuration. The models use 50 hidden neurons.

following parameterization of the recurrent parameters:

$$J^{\text{dyn}} = \gamma \left[\sqrt{1 - r_{\text{str}}^2} \frac{\tilde{S}}{\|\tilde{S}\|_F} + r_{\text{str}} \frac{\tilde{A}}{\|\tilde{A}\|_F} \right], \quad (38)$$

where $\gamma \in \mathbb{R}$ is a learnable global scale.

Using VF and AEP, we train a layered network with one hidden layer of 50 neurons (in which case \tilde{S} and \tilde{A} are block off-diagonal) for different values of r_{str} to investigate the impact of structural asymmetry. We compare two training regimes: training only the input weights J^{in} (and the scale γ), versus training all parameters including J^{dyn} . The first regime trains only the external forces from the input $\rho'(x) \odot J^{\text{in}}u$ (which correspond to a symmetric contribution in the Jacobian) applied to our non-conservative system, while the second additionally trains J^{dyn} and therefore the non-symmetric part of the Jacobian directly.

Figure 3 summarizes the results. We find that AEP maintains robust performance across all asymmetry levels (e.g., achieving an accuracy of $93.8 \pm 0.4\%$ at $r_{\text{str}} = 0$ and $94.9 \pm 0.2\%$ at $r_{\text{str}} = 0.875$ when training all parameters) and can even learn when the recurrent connection matrix J^{dyn} is completely antisymmetric ($r_{\text{str}} = 1$). Additionally, training all parameters shows significant improvement over training only J^{in} .

In contrast, VF performs well at low asymmetry ratios but degrades as asymmetry increases, eventually dropping to chance levels (e.g., accuracies of $5 \pm 3\%$ and $8 \pm 4\%$ at $r_{\text{str}} = 1$ for input-only and all-parameter training, respectively). Interestingly, when we only train J^{in} , VF accuracy collapses around $r_{\text{str}} \approx 0.5$, while when we train all parameters (including the non-conservative part), VF delays this collapse until $r_{\text{str}} \approx 0.8$. Our analysis in Appendix F.2.1 reveals that VF adjusts the dynamics such that the asymmetry of the Jacobian's off-diagonal terms is strictly lower than the

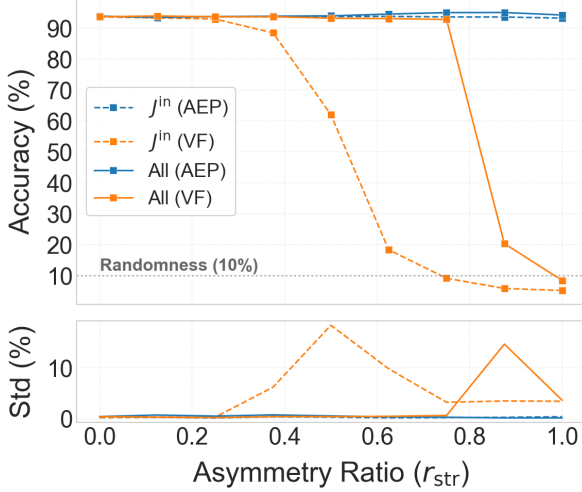


Figure 3. Impact of the structural asymmetry ratio r_{str} on accuracy (top) and standard deviation over 10 runs (bottom). We compare VF (orange) and AEP (blue) under two training regimes: training only J^{in} (dashed) or all parameters (solid).

structural asymmetry ratio. In practice, the training appears to adjust the neuronal state such that neurons connected by strongly asymmetric weights have low activation.

Finally, we confirm in Appendix F.2.1 that AEP learns faster or more efficiently than VF for all levels of asymmetry.

5.3. Feed-Forward Architecture

We now consider the case of a purely feedforward architecture. In this setting, VF trains only the last layer. Indeed, the absence of backward connections prevents the nudging signal applied at the output from propagating to earlier hidden layers. More precisely, for all layers except the last, the stationary states reached under nudging coincide with the free states, resulting in zero weight updates. As only the output layer is trained, the system essentially becomes an Extreme Learning Machine (Huang et al., 2006; Wang et al., 2022).

In contrast, AEP introduces a correction that generates effective backward connections, allowing the nudging signal to influence all layers. We make this explicit for a network with one hidden layer.

Let the state x be partitioned in hidden h and output o layers. The recurrent connection matrix is then :

$$J^{\text{dyn}} = \begin{bmatrix} 0 & 0 \\ W_{h \rightarrow o} & 0 \end{bmatrix}. \quad (39)$$

During the free inference (Eq. 17), the forces acting on the hidden and output layers are:

$$\begin{cases} F_h = \rho'(h) \odot J^{\text{in}} u - h \\ F_o = \rho'(o) \odot W_{h \rightarrow o} \rho(h) - o \end{cases} \quad (40)$$

In contrast, during the nudged phase (Eq. 20), the forces become:

$$\begin{cases} F_h^{\beta} = \rho'(h) \odot (J^{\text{in}} u + (W_{h \rightarrow o})^{\top} (o - \bar{o}^0)) - h \\ F_o^{\beta} = \rho'(o) \odot (W_{h \rightarrow o} \rho(h) - W_{h \rightarrow o} (h - \bar{h}^0)) + \beta \frac{\partial C}{\partial o} - o \end{cases} \quad (41)$$

The force on the hidden layer F_h^{β} now depends on the output layer through the term $\rho'(h) \odot (W_{h \rightarrow o})^{\top} (o - \bar{o}^0)$, enabling the nudge (the term $\beta \frac{\partial C}{\partial o}$) to influence the hidden layer. This implicitly assumes that the hardware implementation supports the physical activation of these backward connections.

As demonstrated in (Scurria, 2026), introducing specific modifications to these methods allows one to recover the exact backpropagation dynamics without approximation.

We validate this using a single hidden layer of only 20 neurons. After training, VF saturates with $64.3 \pm 2.0\%$ accuracy, whereas AEP reaches $92.7 \pm 0.5\%$ accuracy. We expect this discrepancy to increase with network depth, since we increase the number of layers unable to learn under VF. A figure with the accuracy during training can be found in Appendix F.3.2.

6. Discussion and Conclusion

In this work, we extended Equilibrium Propagation (EP) to non-conservative systems that reach stationary states by deriving two mathematically equivalent algorithms that recover the exact gradient of the cost function in the limit of infinitesimal nudging.

The first approach, *Asymmetric EP*, preserves the original inference dynamics. It introduces a corrective force during the nudged phase that remains spatially local, as the anti-symmetric Jacobian is null for unconnected neurons and the perturbation from equilibrium is available at the synapse level. Unlike standard methods like Recurrent Backpropagation (Almeida, 1990; Pineda, 1987), this avoids explicit digital weight transposition. However, the exact mechanism to obtain the local corrective force at the synapse level remains a subject for future work. We also note that AEP shares the temporal non-locality of standard EP.

The second approach, *Dyadic EP*, doubles the state space to map non-reciprocal dynamics onto an energy landscape. Remarkably, this abstract derivation is conceptually reminiscent of multi-compartment cortical neuron models, where distinct cellular compartments process different signals. Specifically, apical dendrites integrate feedback signals (analogous to $z - z'$) separately from basal feedforward inputs (analogous to $z + z'$) (Guerguiev et al., 2017). Additionally, the expanded space allows the positive and negative nudging phases to execute in parallel. This offers a pathway to implement a version of EP that is local in time, with the

trade-off of requiring a doubling of the degrees of freedom on the physical hardware. More fundamentally, the energy defined on the extended state shows that the tools and theoretical guarantees obtained for EP should also apply to the case of non-reciprocal forces, and that the variational principle behind EP is universal in the sense that it can be applied to all networks which operate in a stationary state.

Furthermore, we note that Dyadic EP is not restricted to the EP community and could, for instance, suggest a more physically plausible alternative to the stationary-state Adjoint Method (for fixed inputs) (Chen et al., 2018). Indeed, by solving the forward and adjoint equations simultaneously via relaxation, it circumvents the need for a separate backward-in-time pass.

Finally, our experimental validation on MNIST confirms that AEP consistently outperforms EP and VF. Notably, the method enables effective training of feedforward networks, provided that physical backward pathways can be activated during the augmented phase.

This extension opens new avenues for implementing learning algorithms in neuromorphic hardware, dissipative physical systems, and realistic neural architectures where asymmetry is intrinsic rather than incidental.

Acknowledgments

AES acknowledges financial support by the Horizon Europe Marie Skłodowska-Curie Doctoral Network ‘Postdigital Plus’ (Grant 101169118). DVA acknowledges the support of the French Community of Belgium through a FRIA fellowship. SM acknowledges financial support by the Fonds de la Recherche Scientifique–FNRS, Belgium under EOS Project No. 40007536. Computational resources have been provided by the Consortium des Équipements de Calcul Intensif (CÉCI), funded by the Fonds de la Recherche Scientifique de Belgique (F.R.S.-FNRS) under Grant No. 2.5020.11 and by the Walloon Region.

“ἀρμονίη ἀφανῆς φανερῆς χρείττων”

References

Almeida, L. B. A learning rule for asynchronous perceptrons with feedback in a combinatorial environment. In *Artificial neural networks: concept learning*, pp. 102–111. 1990.

Altmann, L. E., Stern, M., Liu, A. J., and Durian, D. J. Experimental demonstration of coupled learning in elastic networks. *Physical Review Applied*, 22(2):024053, 2024.

Aykroyd, C., Bourgoin, A., and Poncin-Lafitte, C. L. Hamiltonian treatment of non-conservative systems. *arXiv preprint arXiv:2507.18658*, 2025.

Bateman, H. On dissipative systems and related variational principles. *Physical Review*, 38(4):815, 1931.

Berneman, M. and Hexner, D. Equilibrium propagation for periodic dynamics. *arXiv preprint arXiv:2506.20402*, 2025.

Bishop, K. J., Biswal, S. L., and Bharti, B. Active colloids as models, materials, and machines. *Annual Review of Chemical and Biomolecular Engineering*, 14(1):1–30, 2023.

Bowick, M. J., Fakhri, N., Marchetti, M. C., and Ramašwamy, S. Symmetry, thermodynamics, and topology in active matter. *Physical Review X*, 12(1):010501, 2022.

Brandenbourger, M., Locsin, X., Lerner, E., and Coulais, C. Non-reciprocal robotic metamaterials. *Nature communications*, 10(1):4608, 2019.

Cesa-Bianchi, N. and Lugosi, G. *Prediction, learning, and games*. Cambridge university press, 2006.

Chen, R. T., Rubanova, Y., Bettencourt, J., and Duvenaud, D. K. Neural ordinary differential equations. *Advances in neural information processing systems*, 31, 2018.

Cin, N. D., Marquardt, F., and Wanjura, C. C. Training nonlinear optical neural networks with scattering back-propagation. *arXiv preprint arXiv:2508.11750*, 2025.

Costa, P. and Santos, P. A. Directed equilibrium propagation revisited. *Mathematics*, 13(11), 2025. ISSN 2227-7390.

Crick, F. The recent excitement about neural networks. *Nature*, 337, 1989.

Dillavou, S., Stern, M., Liu, A. J., and Durian, D. J. Demonstration of decentralized physics-driven learning. *Physical Review Applied*, 18(1):014040, 2022.

Dillavou, S., Beyer, B. D., Stern, M., Liu, A. J., Miskin, M. Z., and Durian, D. J. Machine learning without a processor: Emergent learning in a nonlinear analog network. *Proceedings of the National Academy of Sciences*, 121(28):e2319718121, 2024.

Ernoult, M., Grollier, J., Querlioz, D., Bengio, Y., and Scellier, B. Updates of equilibrium prop match gradients of backprop through time in an rnn with static input. *Advances in neural information processing systems*, 32, 2019.

Ernoult, M., Grollier, J., Querlioz, D., Bengio, Y., and Scellier, B. Equilibrium propagation with continual weight updates. *arXiv preprint arXiv:2005.04168*, 2020.

Falk, M. J., Strupp, A. T., Scellier, B., and Murugan, A. Temporal contrastive learning through implicit non-equilibrium memory. *Nature Communications*, (16), 2025.

Farinha, M. T., Pequito, S., Santos, P. A., and Figueiredo, M. A. T. Equilibrium propagation for complete directed neural networks. In *Proceedings of the 28th European Symposium on Artificial Neural Networks, Computational Intelligence and Machine Learning (ESANN 2020)*, 2020.

Galley, C. G., Tsang, D., and Stein, L. C. The principle of stationary nonconservative action for classical mechanics and field theories. *arXiv preprint arXiv:1412.3082*, 2014.

Galley, C. R. Classical mechanics of nonconservative systems. *Physical review letters*, 110(17):174301, 2013.

Guerguiev, J., Lillicrap, T. P., and Richards, B. A. Towards deep learning with segregated dendrites. *elife*, 6:e22901, 2017.

Høier, R., Staudt, D., and Zach, C. Dual propagation: accelerating contrastive hebbian learning with dyadic neurons. In *Proceedings of the 40th International Conference on Machine Learning, ICML'23*. JMLR.org, 2023.

Hopfield, J. J. Neural networks and physical systems with emergent collective computational abilities. *Proceedings of the national academy of sciences*, 79(8):2554–2558, 1982.

Huang, G.-B., Zhu, Q.-Y., and Siew, C.-K. Extreme learning machine: theory and applications. *Neurocomputing*, 70 (1-3):489–501, 2006.

Indiveri, G. and Liu, S.-C. Memory and information processing in neuromorphic systems. *Proceedings of the IEEE*, 103(8):1379–1397, 2015.

Kalinin, K. P., Gladrow, J., Chu, J., Clegg, J. H., Cletheroe, D., Kelly, D. J., Rahmani, B., Brennan, G., Canakci, B., Falck, F., et al. Analog optical computer for ai inference and combinatorial optimization. *Nature*, 645(8080):354–361, 2025.

Kendall, J., Pantone, R., Manickavasagam, K., Bengio, Y., and Scellier, B. Training end-to-end analog neural networks with equilibrium propagation. *arXiv preprint arXiv:2006.01981*, 2020.

Laborieux, A. and Zenke, F. Holomorphic equilibrium propagation computes exact gradients through finite size oscillations. *Advances in Neural Information Processing Systems*, 35:12950–12963, 2022.

Laborieux, A. and Zenke, F. Improving equilibrium propagation without weight symmetry through jacobian homeostasis. In *Proceedings of the International Conference on Learning Representations (ICLR) 2024*, Virtual (ICLR), May 2024. doi: 10.48550/arXiv.2309.02214.

Laborieux, A., Ernoult, M., Scellier, B., Bengio, Y., Grollier, J., and Querlioz, D. Scaling equilibrium propagation to deep convnets by drastically reducing its gradient estimator bias. *Frontiers in neuroscience*, 15:633674, 2021.

Laydevant, J., Marković, D., and Grollier, J. Training an ising machine with equilibrium propagation. *Nature Communications*, 15(1):3671, 2024.

LeCun, Y. The mnist database of handwritten digits. <http://yann.lecun.com/exdb/mnist/>, 1998.

Martin, E., Ernoult, M., Laydevant, J., Li, S., Querlioz, D., Petrisor, T., and Grollier, J. Eqspike: spike-driven equilibrium propagation for neuromorphic implementations. *Iscience*, 24(3), 2021.

Massar, S. Equilibrium propagation for learning in lagrangian dynamical systems. *Physical Review E*, 112 (3):035304, 2025.

Massar, S. and Mognetti, B. M. Equilibrium propagation: the quantum and the thermal cases. *Quantum Studies: Mathematics and Foundations*, 12(1):6, 2025.

O'Connor, P., Gavves, E., and Welling, M. Training a spiking neural network with equilibrium propagation. In *The 22nd international conference on artificial intelligence and statistics*, pp. 1516–1523. PMLR, 2019.

Pineda, F. Generalization of back propagation to recurrent and higher order neural networks. In *Neural information processing systems*, 1987.

Pourcel, G., Basu, D., Ernoult, M., and Gilra, A. Lagrangian-based equilibrium propagation: generalisation to arbitrary boundary conditions & equivalence with hamiltonian echo learning. *arXiv preprint arXiv:2506.06248*, 2025.

Rageau, T. and Grollier, J. Training and synchronizing oscillator networks with equilibrium propagation. *Neuromorphic Computing and Engineering*, 2025.

Sajnok, K. and Matuszewski, M. Near-equilibrium propagation training in nonlinear wave systems. *arXiv preprint arXiv:2510.16084*, 2025.

Scellier, B. Quantum equilibrium propagation: Gradient-descent training of quantum systems. *arXiv preprint arXiv:2406.00879*, 2024.

Scellier, B. and Bengio, Y. Equilibrium propagation: Bridging the gap between energy-based models and backpropagation. *Frontiers in computational neuroscience*, 11:24, 2017.

Scellier, B., Goyal, A., Binas, J., Mesnard, T., and Bengio, Y. Generalization of equilibrium propagation to vector field dynamics. *arXiv preprint arXiv:1808.04873*, 2018.

Scellier, B., Mishra, S., Bengio, Y., and Ollivier, Y. Agnostic physics-driven deep learning. *arXiv:2205.15021v1*, 2022.

Scurria, A. E. Backpropagation as physical relaxation: Exact gradients in finite time. In preparation, 2026.

Stern, M., Hexner, D., Rocks, J. W., and Liu, A. J. Supervised learning in physical networks: From machine learning to learning machines. *Physical Review X*, 11(2):021045, 2021.

Wang, J., Lu, S., Wang, S.-H., and Zhang, Y.-D. A review on extreme learning machine. *Multimedia Tools and Applications*, 81(29):41611–41660, 2022.

Wang, Q., Wanjura, C. C., and Marquardt, F. Training coupled phase oscillators as a neuromorphic platform using equilibrium propagation. *Neuromorphic Computing and Engineering*, 4(3):034014, 2024.

Wanjura, C. C. and Marquardt, F. Quantum equilibrium propagation for efficient training of quantum systems based on onsager reciprocity. *Nature Communications*, 16(1):6595, 2025.

Werbos, P. J. Backpropagation through time: what it does and how to do it. *Proceedings of the IEEE*, 78(10):1550–1560, 2002.

Yi, S.-i., Kendall, J. D., Williams, R. S., and Kumar, S. Activity-difference training of deep neural networks using memristor crossbars. *Nature Electronics*, 6(1):45–51, 2023.

A. Gradient Estimation Error in VF

In this appendix, we quantify the gradient estimation error introduced by VF in the limit where the Jacobian asymmetry is small.

Comparing the post-synaptic update terms in Eqs. (12) and (14) gives the following error in the gradient of the cost:

$$\text{Error} = - \left(\frac{\partial F}{\partial \theta}(\bar{x}^0, \theta) \right)^\top \times \left((\mathcal{J}_F(\bar{x}^0, \theta))^{-1} - (\mathcal{J}_F^\top(\bar{x}^0, \theta))^{-1} \right) \frac{\partial C}{\partial x}(\bar{x}^0, y), \quad (42)$$

To quantify this error, we decompose the Jacobian $\mathcal{J}_F(x, \theta)$ into its symmetric part $S\mathcal{J}(x, \theta)$ and antisymmetric part

$$\begin{aligned} S\mathcal{J}(x, \theta) &= \frac{1}{2} (\mathcal{J}_F(x, \theta) + \mathcal{J}_F^\top(x, \theta)), \\ A\mathcal{J}(x, \theta) &= \frac{1}{2} (\mathcal{J}_F(x, \theta) - \mathcal{J}_F^\top(x, \theta)). \end{aligned} \quad (43)$$

Assuming the asymmetry $A\mathcal{J}(x, \theta)$ is small, we can make a series expansion in $S\mathcal{J}^{-1}A\mathcal{J}$ (omitting the dependencies for clarity). Applying the Neumann expansion for small $\|S\mathcal{J}^{-1}A\mathcal{J}\|$ gives

$$(\mathcal{J}_F)^{-1} = \left(\sum_{n=0}^{\infty} (-1)^n (S\mathcal{J}^{-1}A\mathcal{J})^n \right) S\mathcal{J}^{-1}, \quad (44)$$

$$(\mathcal{J}_F^\top)^{-1} = \left(\sum_{n=0}^{\infty} (S\mathcal{J}^{-1}A\mathcal{J})^n \right) S\mathcal{J}^{-1}. \quad (45)$$

Subtracting the two series and assuming convergence, we finally obtain

$$(\mathcal{J}_F)^{-1} - (\mathcal{J}_F^\top)^{-1} = -2 \left(\sum_{n=0}^{\infty} (S\mathcal{J}^{-1}A\mathcal{J})^{2n+1} \right) S\mathcal{J}^{-1}. \quad (46)$$

B. Equivalence between AEP and BPTT

In this appendix, we sketch the equivalence between the gradient estimate computed by AEP and Backpropagation Through Time (BPTT) (Werbos, 2002) for a Recurrent Neural Network with fixed inputs. Our derivation relies on the proof provided by Ernoult et al. (2019), which established that standard (conservative) EP computes gradients identical to those of BPTT. To facilitate direct comparison, we adopt their notation for this section.

A crucial assumption in the proof provided by Ernoult et al. (2019) is that the vector field F (*i.e.*, transition function) derived from a scalar potential function. This implies:

$$\frac{\partial F}{\partial s} = \left(\frac{\partial F}{\partial s} \right)^\top, \quad (47)$$

where s denotes the dynamical state of the system. This symmetry is the linchpin of the equivalence proof, as the gradient expressions derived for BPTT and standard EP differ precisely by a transpose operation applied to $\frac{\partial F}{\partial s}$.

This observation aligns with our analysis in the main text: VF fail in non-conservative systems due to the missing transpose in the post-synaptic term (see Eq. (16)). Following the derivation in Ernoult et al. (2019) (viz., Appendix A, Eqs. (31–33)), the recursive relations for the gradients in BPTT are given by:

$$\nabla_s^{\text{BPTT}}(0) = \frac{\partial \ell}{\partial s}(s_*, y), \quad (48)$$

and for all $t = 1, \dots, K$,

$$\nabla_s^{\text{BPTT}}(t) = \left(\frac{\partial F}{\partial s}(x, s_*, \theta) \right)^\top \nabla_s^{\text{BPTT}}(t-1), \quad (49)$$

$$\nabla_\theta^{\text{BPTT}}(t) = \left(\frac{\partial F}{\partial \theta}(x, s_*, \theta) \right)^\top \nabla_s^{\text{BPTT}}(t-1), \quad (50)$$

where θ represents the optimization parameters, ℓ is the cost function, s_* is the free equilibrium state (satisfying $F(s_*) = 0$), y is the target, and x is the input. The index t denotes the unrolled time steps, initialized at $s(0) = s_*$.

In contrast, the gradients computed by VF follow the recursion (viz., Ernoult et al. (2019), Appendix A, Eqs. (24–26)):

$$\Delta_s^{\text{EP}}(0) = -\frac{\partial \ell}{\partial s}(s_*, y), \quad (51)$$

and for all $t \geq 0$,

$$\Delta_s^{\text{EP}}(t+1) = \frac{\partial F}{\partial s}(x, s_*, \theta) \Delta_s^{\text{EP}}(t), \quad (52)$$

$$\Delta_\theta^{\text{EP}}(t+1) = \left(\frac{\partial F}{\partial \theta}(x, s_*, \theta) \right)^\top \Delta_s^{\text{EP}}(t). \quad (53)$$

Comparing these two sets of equations confirm that the only difference are Eqs. (49) and (52), specifically the transpose of the Jacobian $\frac{\partial F}{\partial s}$ (ignoring the global sign difference in Eqs. (48) and (51)).

In AEP, we modify the dynamics by adding a correction term dependent on the antisymmetric part of the Jacobian. Denoting the force of this augmented system by F^A , the Jacobian at the free equilibrium satisfies:

$$\frac{\partial F^A}{\partial s}(x, s_*, \theta) = \left(\frac{\partial F}{\partial s}(x, s_*, \theta) \right)^\top. \quad (54)$$

By substituting this corrected Jacobian into the recursive relations, AEP recovers the exact transpose required by BPTT. Consequently, our method extends the equivalence between EP and BPTT to the general case of non-conservative force.

C. Proofs for Dyadic EP

We now demonstrate that Dyadic EP correctly trains the parameters θ of the original force field $F(x, \theta)$, giving the exact gradient $\frac{dC(\bar{x}^0)}{d\theta}$ in the limit of infinitesimal nudging.

C.1. Proof of EP

First, recall that standard EP does not strictly require the system to settle at an energy minimum; it requires only that the system reaches a stationary state (a fixed point of the dynamics). Indeed, using the notation of Section 2.1, EP relies on the key identity:

$$\frac{d^2}{d\theta d\beta} E_T(\bar{x}^\beta, \theta) = \frac{d^2}{d\beta d\theta} E_T(\bar{x}^\beta, \theta). \quad (55)$$

Expanding the total derivative with respect to β gives:

$$\begin{aligned} \frac{d}{d\beta} E_T(\bar{x}^\beta, \theta) &= \left(\frac{\partial E_T(\bar{x}^\beta, \theta)}{\partial x} \right)^\top \frac{d\bar{x}^\beta}{d\beta} + \frac{\partial E_T(\bar{x}^\beta, \theta)}{\partial \beta} \\ &= C(\bar{x}^\beta). \end{aligned} \quad (56)$$

Where the first term vanishes because the system is at a stationary state, *i.e.*, $\frac{\partial}{\partial x} E_T(\bar{x}^\beta, \theta) = 0$; this holds even if the point is not a minimum of E_T . Similarly, for the derivative with respect to θ :

$$\frac{d}{d\theta} E_T(\bar{x}^\beta, \theta) = \frac{\partial E_T(\bar{x}^\beta, \theta)}{\partial \theta}, \quad (57)$$

where we additionally assume that the cost function does not depend explicitly on the parameters θ . Substituting these results into Eq. (55) in the limit of infinitesimal nudging ($\beta \rightarrow 0$) recovers the fundamental relation given by Eq. (9).

C.2. Proof of Dyadic EP

Let's go back to Dyadic EP, we analyze the stationary states by introducing the change of variables:

$$m = \frac{z + z'}{2}, \quad d = z - z'. \quad (58)$$

In these coordinates, the augmented energy H_T becomes

$$H_T(m, d, \theta, \beta) = -d^\top F(m, \theta) + \beta C(m) \quad (59)$$

and the dynamic in Eq. (28) can be rewritten as:

$$\frac{dm}{dt} = -\frac{\partial H_T}{\partial d} = F(m, \theta), \quad (60)$$

$$\frac{dd}{dt} = -\frac{\partial H_T}{\partial m} = d^\top J_F(m, \theta) - \beta \frac{\partial}{\partial m} C(m). \quad (61)$$

The stationary states $(\bar{m}^\beta, \bar{d}^\beta)$ are the solutions to:

$$F(\bar{m}^\beta, \theta) = 0, \quad (62)$$

$$\bar{d}^{\beta T} J_F(\bar{m}^\beta, \theta) - \beta \frac{\partial}{\partial m} C(\bar{m}^\beta) = 0. \quad (63)$$

This leads to the following observations:

1) The stationary state of m is independent of β and coincides with the stationary state of the original system:

$$\frac{\bar{z}^\beta + \bar{z}'^\beta}{2} = \bar{m}^\beta = \bar{m}^0 = \bar{x}^0. \quad (64)$$

2) The Jacobian of the extended system defined in Eq. (26) is invertible, provided J_F is invertible. This is most evident from Eq. (61).

3) The stationary state value of d is given by:

$$\bar{d}^\beta = \beta (J_F^\top(\bar{m}^0, \theta))^{-1} \left(\frac{\partial C}{\partial x}(\bar{x}^0) \right) \quad (65)$$

In particular, when $\beta = 0$, we have $\bar{d}^0 = 0$, which implies that the free stationary states coincide: $\bar{z}^0 = \bar{z}'^0$.

4) The cost at the stationary state of the extended system is equal to the cost at the stationary state of the original system:

$$D(\bar{m}^0) = C(\bar{x}^0). \quad (66)$$

Consequently, the gradients of the cost with respect to the parameters are identical.

Since both the original and extended systems, given respectively in Eqs. (28) and (1-2), share the same cost at their respective stationary states, and because the Jacobians of both models are invertible, applying EP update rule to the extended system give the correct gradient estimate for the parameters θ of the original system.

The final step of the proof is to establish the equivalence between the standard parameter update rule in Eq. (8) and the modified rule used by Dyadic EP in Eq. (34). Indeed, if we were to apply the standard update rule in the extended space, the update would be:

$$\Delta\theta \propto -\frac{1}{2\beta} \left(\frac{\partial H(\bar{z}^\beta, \bar{z}'^\beta, \theta)}{\partial \theta} - \frac{\partial H(\bar{z}^{-\beta}, \bar{z}'^{-\beta}, \theta)}{\partial \theta} \right). \quad (67)$$

In Dyadic EP, we instead employ the single-phase update:

$$\Delta\theta \propto -\frac{1}{\beta} \left(\frac{\partial H(\bar{z}^\beta, \bar{z}'^\beta, \theta)}{\partial \theta} \right) \quad (68)$$

This choice avoids the overhead of evolving two coupled equations in the extended space, which would be computationally equivalent to evolving four equations in the original space (two for $+\beta$ and two for $-\beta$). Using Eq. (68), we evolve only one coupled equation for $+\beta$ in the extended space; this corresponds to two equations in the original space, thereby achieving the same computational complexity as AEP. Furthermore, this single-phase formulation suggests a pathway toward making the update local in time,

provided appropriate hardware is used to implement the augmented phase.

Mathematically, these two approaches yield the same gradient estimate, using:

$$\begin{aligned} \frac{\partial H(\bar{z}^\beta, \bar{z}'^\beta, \theta)}{\partial \theta} &= -(\bar{z}^\beta - \bar{z}'^\beta)^\top \frac{\partial F}{\partial \theta} \left(\frac{\bar{z}^\beta + \bar{z}'^\beta}{2}, \theta \right) \\ &= -\beta \left(\frac{\partial F}{\partial \theta}(\bar{z}^0, \theta) \right)^\top (J_F^\top(\bar{z}^0, \theta))^{-1} \\ &\quad \times \left(\frac{\partial C}{\partial x}(\bar{x}^0) \right) + O(\beta^3) \end{aligned} \quad (69)$$

where we have used Eqs. (64) and (65). Inspection of Eq. (69) confirms that, up to corrections of order β^2 , we obtain exactly the same gradient as in AEP.

D. Derivation of the Hopfield-like Energy

In this section, we derive the explicit energy functional for the Continuous Asymmetric Hopfield dynamics defined in Eq. (35). The force field is given by:

$$F(x) = \rho'(x) \odot (J\rho(x)) - x. \quad (70)$$

We omit external inputs J^{in} for brevity, as they appear symmetrically in the Jacobian. The variational Hamiltonian is defined as:

$$H(z, z') = -(z - z')^\top F \left(\frac{z + z'}{2} \right) + \beta C \left(\frac{z + z'}{2} \right). \quad (71)$$

To analyze this expression, we introduce the midpoint $m = \frac{z+z'}{2}$ and the difference $d = z - z'$. Since the separation between z and z' is induced solely by the nudging parameter β , the difference scales as $\|d\| \sim \mathcal{O}(\beta)$. We therefore neglect terms of order $\mathcal{O}(\|d\|^3)$ (i.e., or equivalently $\mathcal{O}(\beta^3)$) as they do not contribute to the gradient of the cost.

The activation at the midpoint can be approximated as:

$$\rho(m) = \frac{\rho(z) + \rho(z')}{2} + \mathcal{O}(\|d\|^2). \quad (72)$$

Similarly, the difference in activations is:

$$\rho(z) - \rho(z') = \rho'(m) \odot d + \mathcal{O}(\|d\|^3). \quad (73)$$

Inverting this relation, we express the state difference as:

$$z - z' = (\rho(z) - \rho(z')) \odot \rho'(m) + \mathcal{O}(\|d\|^3). \quad (74)$$

We substitute these expansions into the interaction term of the Hamiltonian, $H_{\text{int}} = -(z - z')^\top (\rho'(m) \odot J\rho(m))$. Applying the identity $a^\top (b \odot c) = (a \odot b)^\top c$, we obtain:

$$\begin{aligned} H_{\text{int}} &= -((z - z') \odot \rho'(m))^\top J\rho(m) \\ &\approx -(\rho(z) - \rho(z'))^\top J \left(\frac{\rho(z) + \rho(z')}{2} \right). \end{aligned} \quad (75)$$

Expanding the product gives:

$$H_{\text{int}} = -\frac{1}{2} \left[\rho(z)^\top J \rho(z) + \rho(z)^\top J \rho(z') - \rho(z')^\top J \rho(z) - \rho(z')^\top J \rho(z') \right]. \quad (76)$$

We decompose the connectivity matrix J into its symmetric part S and antisymmetric part A . The first and last terms simplify to $\rho(z)^\top S \rho(z)$. The cross terms satisfy:

$$\begin{aligned} \rho(z)^\top J \rho(z') - \rho(z')^\top J \rho(z) &= \rho(z)^\top (J - J^\top) \rho(z') \\ &= \rho(z)^\top (2A) \rho(z'). \end{aligned} \quad (77)$$

Thus, the interaction term reduces to:

$$H_{\text{int}} = -\frac{1}{2} \rho(z)^\top S \rho(z) + \frac{1}{2} \rho(z')^\top S \rho(z') - \rho(z)^\top A \rho(z') + \mathcal{O}(\|d\|^3). \quad (78)$$

Finally, for the nudging term, we expand the cost function around the midpoint:

$$C(m) = \frac{1}{2} (C(z) + C(z')) + \mathcal{O}(\|d\|^2). \quad (79)$$

When multiplying by β , the remainder term becomes $\beta \cdot \mathcal{O}(\|d\|^2)$. Since $\|d\| \sim \mathcal{O}(\beta)$, this remainder is of order $\mathcal{O}(\beta^3)$ and can be consistently discarded alongside the third-order terms from the interaction expansion.

Combining all these components, the final Hamiltonian is:

$$\begin{aligned} H(z, z') &= -\frac{1}{2} \rho(z)^\top S \rho(z) + \frac{1}{2} \rho(z')^\top S \rho(z') \\ &\quad - \rho(z)^\top A \rho(z') + \frac{1}{2} (\|z\|^2 - \|z'\|^2) \\ &\quad + \frac{\beta}{2} (C(z) + C(z')). \end{aligned} \quad (80)$$

The saddle-point dynamics, given by Eq. 32, generated by this Hamiltonian are:

$$\frac{dz}{dt} = \rho'(z) \odot (S \rho(z) + A \rho(z')) - z - \frac{\beta}{2} \frac{\partial C}{\partial z}, \quad (81)$$

$$\frac{dz'}{dt} = \rho'(z') \odot (S \rho(z') + A \rho(z)) - z' + \frac{\beta}{2} \frac{\partial C}{\partial z'}. \quad (82)$$

This system recovers the original continuous Hopfield dynamics when $z = z'$ (assuming $\beta = 0$).

E. Out-of-Equilibrium Mechanics

In this section, we briefly expand on the physical reasoning that motivates the definition of the global energy functional $H(z, z', \theta)$ presented in Eq. (26). Our construction is grounded in the classical mechanics of non-conservative systems, drawing specifically from the formalism developed by (Bateman, 1931; Galley, 2013; Galley et al., 2014).

E.1. The Galley Formalism and the Decomposition

To address non-conservative forces in classical physics, we rely on (Galley, 2013), using a doubled action principle. The general action S on a forward path $z(t)$ and a backward path $z'(t)$ is defined as:

$$S[z, z'] = \int_{t_i}^{t_f} [\mathcal{L}(z, \dot{z}) - \mathcal{L}(z', \dot{z}') + K(z, z')] dt, \quad (83)$$

where \mathcal{L} accounts for the conservative (potential-derived) dynamics, and $K(z, z')$ is a non-conservative potential that couples the two paths.

Ideally, one would decompose the vector field $F(x)$ into a conservative gradient component (associated with \mathcal{L}) and a non-conservative rotational component (K). Mathematically, this is achieved via the **Helmholtz-Hodge decomposition**, which effectively decouples the symmetric and antisymmetric drivers of the dynamics. However, an exact application of this formalism requires evaluating a global integral across the entire domain. In the high-dimensional spaces typical of neural networks, such a calculation is computationally demanding.

E.2. Constructing the Global Energy

Rather than attempting to isolate a conservative potential, we treat the *entire* vector field $F(x, \theta)$ as a generalized non-conservative force.

We propose to construct a single global interaction energy H , used also by (Galley et al., 2014), that embeds the full vector field F directly into the bilinear coupling term between the doubled variables $z, z' \in \mathbb{R}^n$:

$$H(z, z', \theta) = -(z - z')^\top F \left(\frac{z + z'}{2}, \theta \right). \quad (84)$$

This specific bilinear form is designed to act as a *generator* for the complete vector field F , rendering the explicit decomposition unnecessary. We prescribe the equations of motion as a saddle-point flow on this energy (Eq. 32):

$$\frac{dz}{dt} = -\frac{\partial H}{\partial z}, \quad \frac{dz'}{dt} = \frac{\partial H}{\partial z'}. \quad (85)$$

Evaluating these gradients yields the explicit free dynamics:

$$\frac{dz}{dt} = F(m) + \frac{1}{2} [\mathcal{J}_F(m)]^\top (z - z'), \quad (86)$$

$$\frac{dz'}{dt} = F(m) - \frac{1}{2} [\mathcal{J}_F(m)]^\top (z - z'), \quad (87)$$

where $m = \frac{1}{2}(z + z')$.

On the physical submanifold where $z = z'$ (i.e., zero difference $d = 0$), the coupling terms containing $[\mathcal{J}_F]^\top (z - z')$

vanish identically. On this manifold, both equations collapse to the exact target dynamics:

$$\frac{dz}{dt} = F(z, \theta), \quad \frac{dz'}{dt} = F(z', \theta). \quad (88)$$

This formulation allows us to apply the doubled-variable framework to arbitrary differentiable dynamical systems without requiring the prohibitive Hodge decomposition.

E.3. Symmetry Breaking as Credit Assignment

The variational principle established above successfully generates the inference dynamics on the diagonal manifold $z = z'$. On this manifold, the system possesses a gauge symmetry: the second variable z' is redundant, and the difference $d = z - z'$ is zero.

We propose to exploit this symmetry to perform credit assignment. Specifically, we introduce the task cost $D(z, z') = C(\frac{z+z'}{2})$ as a symmetry-breaking potential. By adding this cost to the global energy (forming $H_T = H + \beta D$), we intentionally perturb the gauge symmetry of the system.

This perturbation exerts opposite forces on the pair: the task cost pushes z and z' in opposite directions. This induces a physical separation $d \neq 0$. The evolution of this difference variable follows the difference of the velocity fields. In the limit of small β (where the system remains close to the *free equilibrium* $m \approx \bar{x}^0$), the dynamics become:

$$\frac{dd}{dt} = \frac{dz}{dt} - \frac{dz'}{dt} = [\mathcal{J}_F(\bar{x}^0)]^\top d - \beta \nabla C(\bar{x}^0). \quad (89)$$

This naturally recovers the exact stationary-state adjoint equation required for gradient computation. Thus, in our framework, EP emerges not as a heuristic, but as the physical relaxation of the stress induced by explicitly breaking the symmetry of the inference dynamics.

F. Experimental Details

As in the main text, the neuronal dynamics are governed by the vector field:

$$F_i = \rho'(x_i) \left(\sum_j J_{ij}^{\text{dyn}} \rho(x_j) + b_i(u) \right) - x_i, \quad (90)$$

where the input-dependent bias $b_i(u)$ is precomputed for each MNIST input u as:

$$b_i(u) = \sum_{l \in \text{in}} J_{il}^{\text{in}} u_l. \quad (91)$$

This term projects the input space into the recurrent subspace. The bias yields a diagonal contribution to the Jacobian $\mathcal{J}_F = \frac{\partial F}{\partial x}$, and therefore does not contribute to the

antisymmetric correction used in the augmented dynamics (20) of AEP.

The input parameters are then updated using the standard learning rule (21). In particular, the presynaptic term associated with the input weights is given by,

$$\frac{\partial F_i}{\partial J_{kl}^{\text{in}}} = \delta_{ik} \rho'(x_i) u_l. \quad (92)$$

The presynaptic terms associated with the dynamical parameters J_{ij}^{dyn} depend on the experiment.

F.1. Symmetric Initialization

F.1.1. LEARNING RULES

For clarity, we write the learning rules for VF and AEP. For the input weights, using (92), give directly:

$$\Delta J_{ik}^{\text{in}} \propto \frac{1}{2\beta} \left[(\bar{x}_i^{+\beta} - \bar{x}_i^{-\beta}) \rho'(\bar{x}_i^0) u_k \right], \quad (93)$$

while for the recurrent weight, we get:

$$\Delta J_{ij}^{\text{dyn}} \propto \frac{1}{2\beta} \left[(\bar{x}_i^{+\beta} - \bar{x}_i^{-\beta}) \rho'(\bar{x}_i^0) \rho(\bar{x}_j^0) \right]. \quad (94)$$

For EP, we directly get:

$$\Delta J_{ik}^{\text{in}} \propto \frac{1}{2\beta} \left[\left(\rho(\bar{x}_i^{+\beta}) - \rho(\bar{x}_i^{-\beta}) \right) u_k \right], \quad (95)$$

and for the recurrent weights:

$$\Delta J_{ij}^{\text{dyn}} \propto \frac{1}{2\beta} \left[\rho(\bar{x}_i^{+\beta}) \rho(\bar{x}_j^{+\beta}) - \rho(\bar{x}_i^{-\beta}) \rho(\bar{x}_j^{-\beta}) \right]. \quad (96)$$

F.1.2. SUPPLEMENTARY NUMERICAL RESULTS

To complement Fig. 2, we report the evolution of the accuracy of the three methods in Fig. 4. We consider a layered network with 50 hidden neurons; while this capacity is insufficient for state-of-the-art performance, it amplifies the difference in accuracy between models to aid visualization. Models are trained for 20 epochs starting from a symmetric configuration, the natural setting for both VF and EP. As expected, with this initialization, AEP consistently outperforms the other methods and learns faster by exploiting the additional degrees of freedom of the asymmetric network.

F.2. Fixed Asymmetry Ratio

This section details the implementation for the fixed asymmetry ratio experiments presented in Section 5.2, followed by complementary numerical results regarding learning speed and induced Jacobian asymmetry.

Parameter	Sym. Init. / Feedforward	Fixed r_{str}
Learning Rate (Input-Hidden)	0.05	0.05
Learning Rate (Hidden-Output)	0.01	0.01
Time Step (Dynamics Integration)	0.5	0.3
Nudging Parameter (β)	0.5	0.5
Free-phase Steps (n_{free})	20	30
Nudged-phase Steps (n_{nudge})	10	10
Repetitions (for averaging)	10	10
Number of Epochs	40 / 20	30
Batch Size	64	64
Scaling Parameter γ	n.a.	$\sqrt{60}$
Layer Structure	784 - n.a. - 10	784-50-10
Activation function ρ	tanh	tanh
Initial Recurrent State s	$s \sim \mathcal{U}(-1, 1)$	$s \sim \mathcal{U}(-1, 1)$
Initial Parameters θ	$\theta \sim \mathcal{N}(0, \frac{1}{N})$	$\theta \sim \mathcal{N}(0, \frac{1}{N})$
Number of Runs (training + inference)	10	10

Table 1. Trained Model Hyperparameters. N is the total number of neurons, $\mathcal{U}(-1, 1)$ is a uniform distribution, and $\mathcal{N}(\mu, \sigma^2)$ is a Gaussian distribution. For the r_{str} parametrization, we choose more cautious hyperparameters for training and inference compared to the symmetric initialization, due to increasingly non-conservative and potentially oscillatory dynamics.

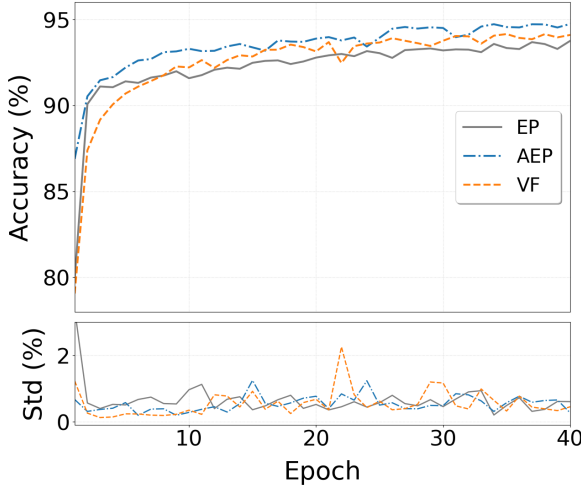


Figure 4. Evolution of the mean accuracy and standard deviation (over 10 runs) during training on MNIST for AEP, EP, and VF. Models use 50 hidden neurons.

F.2.1. LEARNING RULES

Parametrization and notation. To enforce a fixed asymmetry ratio, we explicitly parameterize the independent elements of Eq. (38). We introduce two parameter vectors θ^S and θ^A of size $M = N_{\text{dyn}}(N_{\text{dyn}} - 1)/2$, which encode the off-diagonal elements of the symmetric and antisymmetric components \tilde{S} and \tilde{A} , respectively. The correspondence between matrix and vector indices is given by:

$$k(i, j) = \frac{(i-1)(i-2)}{2} + j, \quad (1 \leq j < i \leq N_{\text{dyn}}) \quad (97)$$

where the condition $j < i$ selects the strictly lower triangular elements. Introducing an additional vector ξ for the diagonal elements of \tilde{S} , the full matrix are constructed as:

$$\tilde{S}_{ij} = \delta_{ij}\xi_i + (1 - \delta_{ij})\theta_{k(\max(i,j),\min(i,j))}^S, \quad (98)$$

$$\tilde{A}_{ij} = \epsilon_{ij}\theta_{k(\max(i,j),\min(i,j))}^A, \quad (99)$$

where ϵ_{ij} is the Levi-Civita symbol. The dynamical parameters are then given by:

$$J_{ij}^{\text{dyn}} = \gamma(c_S \tilde{S}_{ij} + c_A \tilde{A}_{ij}), \quad (100)$$

with normalization coefficients

$$c_S = \frac{\sqrt{1 - r_{\text{str}}^2}}{F_S}, \quad c_A = \frac{r_{\text{str}}}{F_A}, \quad (101)$$

defined in terms of the Frobenius norms:

$$F_S = \sqrt{\sum_{i=1}^N \xi_i^2 + 2 \sum_{k=1}^M (\theta_k^S)^2}, \quad (102)$$

$$F_A = \sqrt{2 \sum_{k=1}^M (\theta_k^A)^2}. \quad (103)$$

Presynaptic computation. The dependence of the normalization coefficients on the parameters introduces additional regularization terms in the learning rule compared to the parameterization of (Scellier & Bengio, 2017). The

gradients of the normalization coefficients are:

$$\frac{\partial c_S}{\partial \theta_k^S} = -2c_S \frac{\theta_k^S}{(F_S)^2}, \quad \frac{\partial c_S}{\partial \xi_m} = -c_S \frac{\xi_m}{(F_S)^2}, \quad (104)$$

$$\frac{\partial c_A}{\partial \theta_k^A} = -2c_A \frac{\theta_k^A}{(F_A)^2}. \quad (105)$$

Combining these with the derivatives of the matrices \tilde{S} and \tilde{A} :

$$\frac{\partial \tilde{S}_{ij}}{\partial \theta_k^S} = \delta_{ip}\delta_{jq} + \delta_{iq}\delta_{jp}, \quad \frac{\partial \tilde{S}_{ij}}{\partial \xi_k} = \delta_{ij}\delta_{kj} \quad (106)$$

$$\frac{\partial \tilde{A}_{ij}}{\partial \theta_k^A} = \delta_{ip}\delta_{jq} - \delta_{iq}\delta_{jp}, \quad (107)$$

where k corresponds to the index pair (p, q) with $p > q$, as defined in Eq. (97). The full presynaptic terms are then:

- For the diagonal parameters ξ_m :

$$\frac{\partial F_i}{\partial \xi_m} = \gamma c_S \rho'(x_i) \left[-\frac{\xi_m}{(F_S)^2} \sum_{j=1}^N \tilde{S}_{ij} \rho(x_j) + \delta_{im} \rho(x_m) \right]. \quad (108)$$

- For the off-diagonal symmetric parameters θ_k^S (where $p > q$):

$$\frac{\partial F_i}{\partial \theta_k^S} = \gamma c_S \rho'(x_i) \left[-2 \frac{\theta_k^S}{(F_S)^2} \sum_{j=1}^N \tilde{S}_{ij} \rho(x_j) + \delta_{ip} \rho(x_q) + \delta_{iq} \rho(x_p) \right]. \quad (109)$$

- For the off-diagonal antisymmetric parameters θ_k^A (where $p > q$):

$$\frac{\partial F_i}{\partial \theta_k^A} = \gamma c_A \rho'(x_i) \left[-2 \frac{\theta_k^A}{(F_A)^2} \sum_{j=1}^N \tilde{A}_{ij} \rho(x_j) + \delta_{ip} \rho(x_q) - \delta_{iq} \rho(x_p) \right]. \quad (110)$$

Initialization. To ensure the stability of the system, we initialize our parameters such that the variance of dynamical parameters scales as $\text{Var}[J_{ij}^{\text{dyn}}] \propto 1/N_{\text{dyn}}$. This is a conservative choice for the layered architectures used in our experiments, where many entries of J_{ij}^{dyn} are zero.

In practice, we initialize the parameter vectors θ^S, θ^A , and ξ with identical variances σ^2 . For large N_{dyn} , the expected

Frobenius norms approximate to $\mathbb{E}[F_{S,A}] \approx N_{\text{dyn}}\sigma$. Consequently, the normalization coefficients become:

$$c_S \approx \frac{\sqrt{1 - r_{\text{str}}^2}}{N_{\text{dyn}}\sigma}, \quad c_A \approx \frac{r_{\text{str}}}{N_{\text{dyn}}\sigma}. \quad (111)$$

Since the symmetric and antisymmetric components are statistically independent, the variance of the weights is derived as follows:

- Diagonal elements ($i = j$):

$$\text{Var}[J_{ii}^{\text{dyn}}] = \gamma^2 c_S^2 \sigma^2 \approx \gamma^2 \frac{1 - r_{\text{str}}^2}{N_{\text{dyn}}^2}. \quad (112)$$

- Off-diagonal elements ($i \neq j$):

$$\text{Var}[J_{ij}^{\text{dyn}}] = \gamma^2 (c_S^2 + c_A^2) \sigma^2 \approx \frac{\gamma^2}{N_{\text{dyn}}^2}, \quad (113)$$

To satisfy $\text{Var}[J_{ij}^{\text{dyn}}] \propto 1/N_{\text{dyn}}$, we set:

$$\gamma = \sqrt{N_{\text{dyn}}} \quad (114)$$

Note that by random matrix theory, diagonal elements do not affect stability in the large N_{dyn} limit.

Simplification. Although the parameterization above is fully general, a simpler construction is possible by removing self-connections ($\xi = 0$) and enforcing identical parameterization for the symmetric and antisymmetric components, *i.e.*, $\theta^S = \theta^A = \theta$. The matrix elements then become:

$$\tilde{S}_{ij} = (1 - \delta_{ij})\theta_{k(\max(i,j),\min(i,j))}, \quad (115)$$

$$\tilde{A}_{ij} = \epsilon_{ij}\theta_{k(\max(i,j),\min(i,j))}. \quad (116)$$

In this case, the Frobenius norms are equal ($F_S = F_A$), and we can omit the explicit normalization:

$$J_{ij}^{\text{dyn}} = \sqrt{1 - r_{\text{str}}^2} \tilde{S}_{ij} + r_{\text{str}} \tilde{A}_{ij}. \quad (117)$$

For a parameter θ_k corresponding to indices (p, q) with $p > q$, the presynaptic term is given by:

$$\frac{\partial F_i}{\partial \theta_k} = \rho'(x_i) \left[\left(\sqrt{1 - r_{\text{str}}^2} + r_{\text{str}} \right) \delta_{ip} \rho(x_q) + \left(\sqrt{1 - r_{\text{str}}^2} - r_{\text{str}} \right) \delta_{iq} \rho(x_p) \right]. \quad (118)$$

While this parameterization works in simulations and keeps the number of parameters constant for all r_{str} , it constrains the asymmetry to be “homogeneous”, by which we mean that the asymmetry ratio is identical for every pair of neurons; hence, the network cannot learn to be symmetric in one region and antisymmetric in another. Therefore, we choose to explore the more general case of (38) in our experiments.

F.2.2. SUPPLEMENTARY NUMERICAL RESULTS

To complement the results of Fig 3, we analyze the training efficiency as a function of the asymmetry ratio r_{str} and investigate the robustness of VF by monitoring the Jacobian asymmetry.

Training efficiency. We first study the training efficiency of the two algorithms as a function of the asymmetry ratio r_{str} . Inspired by the related concept in (Cesa-Bianchi & Lugosi, 2006), we define the cumulative loss as the accumulated difference between the free equilibrium cost and a zero-cost baseline (perfect prediction) during learning. Specifically, for each method and value of r_{str} , we calculate the cumulative loss by summing the batch-averaged costs of the first 5 epochs (out of 30, to avoid saturation effects), and reporting the mean and standard deviation over 10 independent training runs. Mathematically, for each run:

$$\text{Cumul. Loss} = \sum_{\text{epoch}=1}^5 \sum_{k=1}^{N_{\text{batches}}} \left(\sum_{(\bar{x}^0, u) \in \mathcal{B}_k} \frac{C(\bar{x}^0, u)}{|\mathcal{B}_k|} \right), \quad (119)$$

where \mathcal{B}_k represents the k -th batch, and $|\mathcal{B}_k|$ denotes the number of examples in the batch. The parameters are updated after each batch step; consequently, the free equilibrium \bar{x}^0 is inferred using the updated parameters and the current example u .

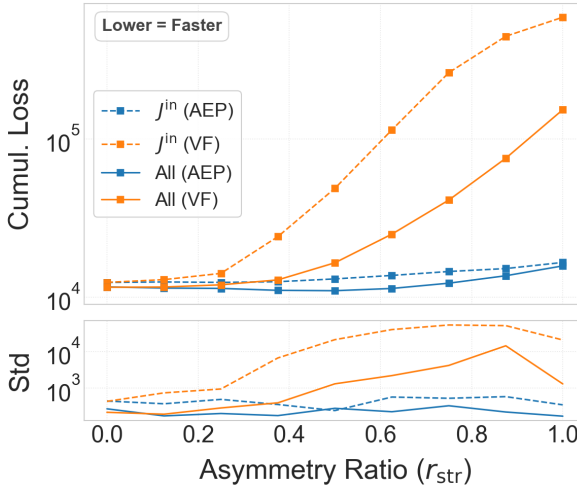


Figure 5. Cumulative loss as defined by (119) over the first 5 epochs of training, for different asymmetry ratios r_{str} . We compare VF (orange) and AEP (blue), under two training regimes: training only j^{in} (dashed) or all parameters (solid).

In Fig 5, we observe that learning slows down for both algorithms when $r_{\text{str}} \gtrsim 0.6$. This behavior likely results from the increased difficulty of reaching a stationary state as the dynamics become strongly asymmetric. With a fixed number of inference steps, incomplete convergence degrades the accuracy of the gradient estimates, thereby slowing down

the learning. Additionally, while VF can eventually achieve competitive accuracy, it is consistently slower than AEP as soon as asymmetry is introduced.

Jacobian asymmetry. We next examine how the structural asymmetry r_{str} is reflected in the Jacobian of the dynamics (35), given by:

$$\begin{aligned} \frac{\partial F_i}{\partial s_j} = & (1 - \delta_{ij}) \rho'(x_i) J_{ij}^{\text{dyn}} \rho'(x_j) \\ & + \delta_{ij} \left[\rho'(x_i) (J_{ii}^{\text{dyn}} \rho'(x_i)) + \rho''(x_i) b_i - 1 \right]. \end{aligned} \quad (120)$$

In our layered architecture, the self-connections are zero ($J_{ii}^{\text{dyn}} = 0$). For the following analysis, we neglect all diagonal terms in the Jacobian (including external inputs and potential), since they do not contribute to the antisymmetric correction (20) and thus to the discrepancy between the performance of VF and AEP. Consequently, we define the following asymmetry ratio based solely on the off-diagonal Jacobian $\mathcal{J}_{F,\text{off}}$:

$$r_{\text{jac}} = \frac{\|\mathcal{J}_{F,\text{off}} - \mathcal{J}_{F,\text{off}}^{\top}\|_F}{\|\mathcal{J}_{F,\text{off}}\|_F}, \quad (121)$$

The results are presented in Fig 6. For each trained model and ratio r_{str} , we compute r_{jac} averaged over the stationary states of the first batch (64 images) across 10 independent runs. We observe that when structural asymmetry is strong and all parameters are trained, VF partially compensates for the asymmetry by adjusting the neuronal states. This can be understood by rewriting the ratio as:

$$r_{\text{jac}} = \frac{\left\| \rho'(x_i) \left(J_{ij}^{\text{dyn}} - (J_{ji}^{\text{dyn}})^{\top} \right) \rho'(x_j) \right\|_F}{\left\| \rho'(x_i) J_{ij}^{\text{dyn}} \rho'(x_j) \right\|_F}. \quad (122)$$

Compared to the structural asymmetry ratio in Eq. (37), a value of $r_{\text{jac}} < r_{\text{str}}$ indicates that the neuronal states effectively dampen the structural asymmetry, rendering the dynamics more symmetric. This symmetrization of the Jacobian appears without imposing an additional symmetrization penalty and could be enhanced using the method of (Laborieux & Zenke, 2022). This mechanism likely explains the superior performance of ‘All (VF)’ compared to ‘ j^{in} (VF)’ in Fig 3, as the former is able to use the additional degrees of freedom to reduce the effective asymmetry at high r_{str} .

F.3. Feedforward Network

F.3.1. LEARNING RULES

For clarity, we write the learning rules for VF and AEP in this layered architecture using the notation of Section 5.3.

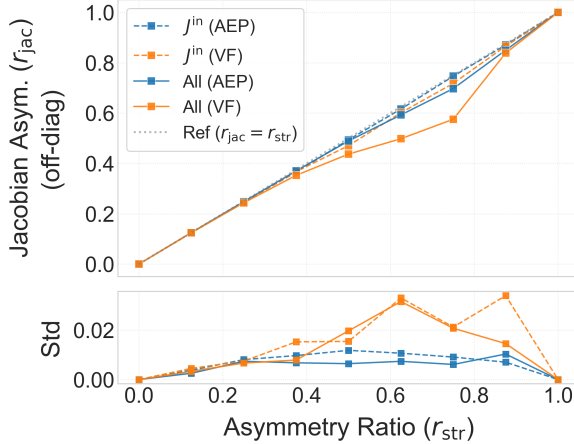


Figure 6. Asymmetry ratio of the Jacobian r_{jac} defined in equation (121) after training for different asymmetry ratios r_{str} . We compare VF (orange) and AEP (blue), under two training regimes: training only J^{in} (dashed) or all parameters (solid).

For the input weights connecting to the hidden layer, we get the usual formula:

$$\Delta J_{ik}^{\text{in}} \propto \frac{1}{2\beta} \left[(\bar{h}_i^{+\beta} - \bar{h}_i^{-\beta}) \rho'(\bar{h}_i^0) u_k \right], \quad (123)$$

while for the feedforward weights connecting the hidden to the output layer, we get:

$$\Delta(W_{h \rightarrow o})_{ji} \propto \frac{1}{2\beta} \left[(\bar{o}_j^{+\beta} - \bar{o}_j^{-\beta}) \rho'(\bar{o}_j^0) \rho(\bar{h}_i^0) \right]. \quad (124)$$

Note that EP is not applicable in this case.

F.3.2. SUPPLEMENTARY NUMERICAL RESULTS

In addition to the final accuracy reported in Sec. 5.3, we show in Fig. 7 the evolution of the accuracy over 20 epochs for AEP and VF.

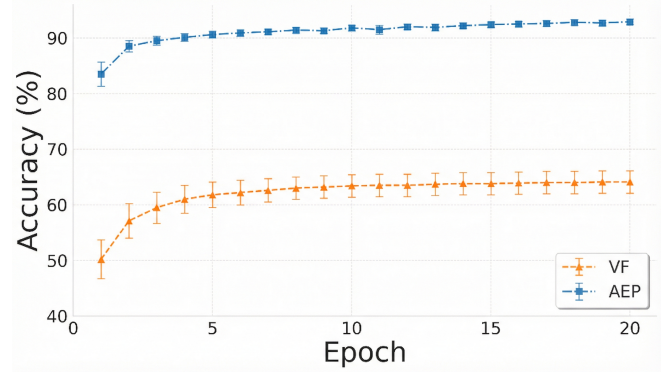


Figure 7. Comparison of AEP and VF on a feedforward network. Test accuracy on MNIST is shown as a function of training epochs for a single-hidden-layer network with 20 neurons. Curves report the mean and standard deviation over 10 runs. Best accuracies are $92.7\% \pm 0.5\%$ (AEP) and $64.3\% \pm 2.0\%$ (VF).